Microstructure and Loading Effects on Fatigue Crack Growth Paths in Engineering Alloys

Anastasios G. Gavras and Diana A. Lados

Integrative Materials Design Center
Worcester Polytechnic Institute, USA

Abstract

Fatigue crack growth is a critical consideration in designing structural materials and components subjected to dynamic loading. In this work, a novel design approach has been developed bridging the framework of fracture mechanics and damage tolerance to materials fundamentals. Extensive fatigue crack growth testing, fractography, and modeling have been performed on various structural materials to create and validate the developments. Focus was given to the influence of both microstructure and initial flaw size on fatigue crack growth. First, a new methodology for predicting the response of microstructurally small cracks in the near-threshold regime will be presented and discussed. Next, two-parameter maps that link loading conditions to the microstructural characteristic response at various crack growth stages have been constructed and will be introduced as tools for materials optimization. Examples of integrating materials knowledge into structural design for fatigue crack growth performance will be given.

Keywords: long and small fatigue crack growth, microstructure, crack length

1 INTRODUCTION

Damage tolerance has been extensively used in component design, especially in aerospace applications, since the 1970s. Original work by Paris et al. [1] showed that fracture mechanics principles can be utilized in fatigue to calculate the structural life. The initial life predictions were made based on long fatigue crack growth data, however the anomalous behavior of small fatigue cracks relative to long cracks was observed [2], and has been puzzling the community for nearly four decades.

The so-called *small crack effect* was clearly documented by Suresh et al. [3], and since then, it has been an important consideration in design. In spite of its significant role, it needs to be noted that other types of fatigue crack growth data (e.g. long, short) can be useful in design when the initial flaws are comparable to relevant microstructural scales. In most cases though, cracks start small and the use of small fatigue crack growth data in design is appropriate.

Various models have been proposed to predict the behavior of small fatigue cracks. Some of them rely on the use of microstructural fracture mechanics [4], while others approach the small crack problem through several linear-elastic fracture mechanics (LEFM) modifications [5-9]. For instance, high stress ratio, R, long fatigue crack growth data were used to approximate the behavior of small fatigue cracks [5] since at high R the

closure levels for long cracks decrease to those experienced by small cracks. In addition, other researchers adjusted the fatigue crack tip driving force for small cracks based on crack closure and plasticity [6]. El Haddad et al. [7] incorporated a crack length term, a_o, into the calculated ΔK for long cracks to capture small crack effects. Frost and Dugdale [8] introduced an empirical method to correlate the growth rates of long and small fatigue cracks without invoking fracture mechanics. This approach was recently used by Caton et al. [9] for the description of small fatigue crack growth in cast aluminum alloys.

Murakami et al. [10] developed a simple methodology to predict the threshold stress intensity factor range, ΔK_{th}, of materials containing notches and defects of varying geometry. Based on the observation that the maximum stress intensity factor, K_{max}, is proportional to the square root of crack area for different geometries of defects, they proposed that the threshold stress intensity factor range, ΔK_{th}, is a function of the square root of the crack area and micro-hardness of the material. Most of these approaches are empirical and do not take into account the material's characteristic microstructural features.

In this study, a new model that predicts the response of microstructurally small fatigue cracks was developed by combining fracture mechanics with materials science. The effects of the materials microstructure on fatigue crack growth at various growth stages were also examined and two-parameter maps relating loading conditions to microstructural damage were constructed.

2 EXPERIMENTAL PROCEDURE

2.1 Materials and Heat Treatment

Fatigue crack growth behavior in cast A535 and wrought 6061 aluminum alloys, and wrought Ti-6Al-4V alloys, was investigated in this study. The microstructures of the alloys were adjusted to represent conditions encountered in actual applications. A cast A535 alloy with coarse grain structure was prepared and studied in the as-cast condition, Fig. 1(a). A 6061 rolled plate was used in the T6 temper. The grain structure of the 6061-T6 alloy consists of recrystallized "pancake" grains, as shown in Fig. 1(b). The Ti-6Al-4V alloys were used in beta- and mill-annealed heat treating conditions, resulting in lamellar and globular morphology of the alpha phase in the beta matrix, Figs. 1(c,d). For the wrought alloys, all specimens were extracted from the longitudinal-transverse (L-T) plane.

2.2 Fatigue Crack Growth Testing

Long fatigue crack growth experiments were conducted using compact tension, C(T), specimens. C(T) specimens with 50.8 mm (2 in) width (W) and 10.2 mm (0.4 in) thickness (B) were machined according to the ASTM-E647 standard [11]. Overall C(T) specimen dimensions were 63.5 mm x 61 mm x 10.2 mm (2.5 in x 2.4 in x 0.4 in). The initiation notch length (measured from the front face) was 25.4 mm (1 in). The notch was introduced using wire-cut electrical discharge machining (EDM) and its thickness was 0.254 mm (0.01 in). Sufficient material was removed during sample preparation to ensure minimal residual stresses in the final fatigue crack growth testing specimens.

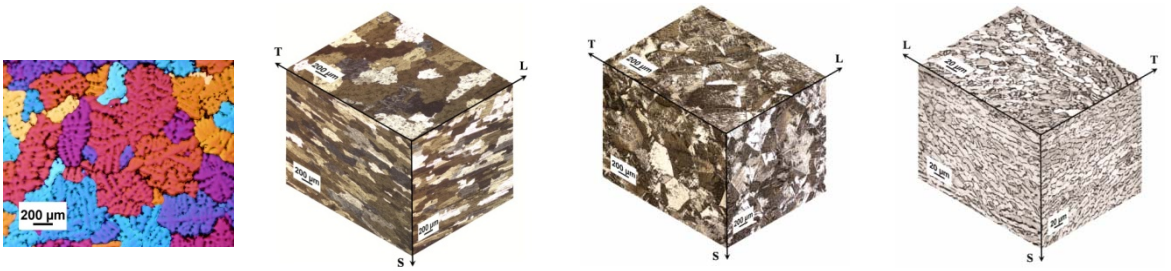

Grain size: 450 µm

Grain size:
183 µm x 551 µm

Prior-β grain size: 600 µm
α colony size: 100-140 µm
α lath width: 1 µm
α (hcp): 61%
β (bcc): 39%

α grain size: 13 µm
α (hcp): 69%
β (bcc): 31%

(a) (b) (c) (d)

Figure 1: Grain structure of (a) cast A535-F, (b) wrought 6061-T6, (c) beta-annealed Ti-6Al-4V, and (d) mill-annealed Ti-6Al-4V. *Note:* (a) Optical micrograph from specimen electrolytically etched with Barkers reagent (3% HFB_4) at 35 V for 120 seconds (polarized light). (b) Optical micrograph from specimen electrolytically etched with Barkers reagent (3% HFB_4) at 30 V for 180 seconds (polarized light). (c,d) Optical micrographs from specimens etched with oxalic reagent (20 ml HF, 20 g $H_2C_2O_4$, and 98 ml H_2O) for 15 seconds.

Constant stress ratio tests at R=0.1, 0.5, and 0.7 were performed in air at room temperature, 22-24˚C (71-75˚F), and relative humidity of 20-50%. These tests were run under K control at a cyclic frequency of 20 Hz in order to generate data in Regions I and II. Specifically, a K gradient of -0.19/mm (-5/in) was used for the decreasing K part of the test to determine the crack growth threshold value, ΔK_{th}. Region II data were generated during increasing K tests with a K gradient of +0.19/mm (+5/in). The final part of the tests was run at constant load at a cyclic frequency of 5 Hz to generate data in Region III of fast crack growth.

Small fatigue crack growth experiments were performed on corner flaw tension, CF(T), and surface flaw tension, SF(T), specimens. The specimens had a gage cross-section of 10.2 mm x 5.1 mm (0.4 in x 0.2 in). The initial notch size varied from 75 µm to 300 µm depending on the size of the material's characteristic microstructure. Wire-cut electrical discharge machining (EDM) and a knife-edge were used to introduce surface and corner flaws, respectively. All small fatigue crack growth tests were run at constant R=0.1 and cyclic frequency of 20 Hz. The direct current potential drop (DCPD) method was used to measure crack length. Testing was done at room temperature, 22-24˚C (71-75˚F), and relative humidity of 20-50%.

3 RESULTS AND DISCUSSION

3.1 A Novel Methodology to Predict Microstructurally Small Fatigue Crack Growth

An original methodology was developed to predict the microstructurally small fatigue crack growth response in two steps, starting from long fatigue crack growth data. The two steps are schematically shown in Fig. 2.

Figure 2: Schematic representation of the two steps followed in the proposed methodology.

In the first step, the physically small fatigue crack growth response is predicted from experimental long fatigue crack growth data. The primary difference between long and physically small fatigue cracks is the shielding zone behind the crack tip, which gives rise to closure [12]. Closure effects were removed from long fatigue crack growth data using the Adjusted Compliance Ratio, *ACR*, method [13]. In addition, a data-reduction prediction process was introduced to generate physically small and long fatigue crack growth data at any positive stress ratio, *R*, by considering the K_{max} sensitivity and the long crack closure levels, Fig. 3.

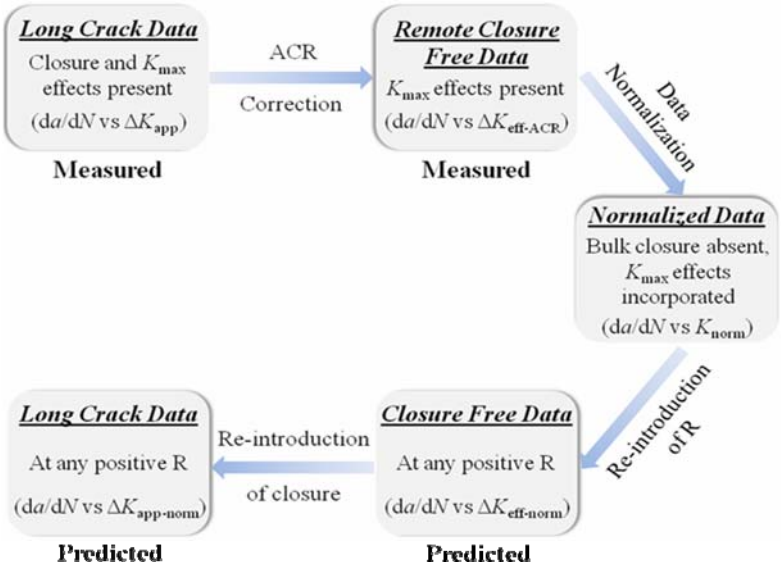

Figure 3: Schematic illustration of the data-reduction prediction steps.

In Fig. 4 it is shown that although predicted closure free data are in good agreement with the experimental physically small fatigue crack growth data (right), microstructurally small crack effects are not captured (left). This observation set the basis for the development of a corrective model that accounts for microstructurally small crack growth effects, in the second step. A simplified expression of the model is shown in Eq. (1):

$$\Delta K_{microstructurally-small} = \Delta K_{physically-small} \times \Omega = K_{norm} \times (1 - R)^n \times \Omega \quad (1)$$

Prior to describing the proposed model and the microstructural term, Ω, the assumptions of this model need to be stated. These are:

- The "breakdown" of the similitude concept is accepted for the purpose of quantifying the differences between long and small fatigue crack growth data. The similitude concept states that two cracks, regardless of their size, will behave in an identical manner when they are subjected to the same stress intensity, *K* [14].

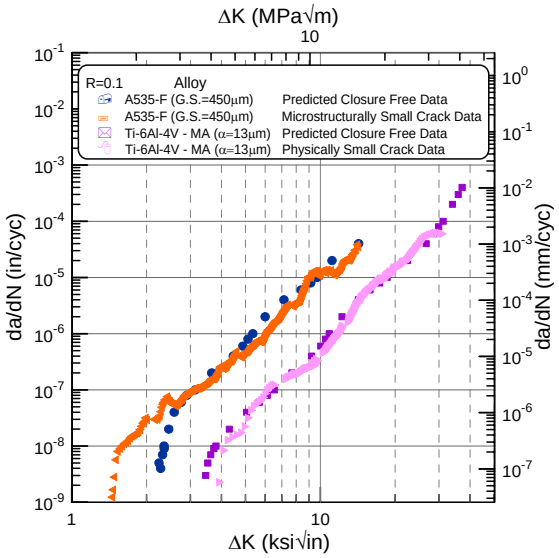

Figure 4: Comparison between predicted closure free data and experimental physically and microstructurally small crack growth data for Al and Ti alloys at R=0.1.

- The cracks are atomistically sharp. Thus, crack growth can be modeled in a two dimensional domain.
- The resolved component of the applied stress has exceeded the critical value necessary for crack propagation.

The Ω term is microstructure dependent and a function of crack length, a, local and bulk properties, and areas of characteristic microstructural features, Eq. (2). It consists of two terms, the crack length term and the property term:

$$\Omega = \frac{a_{initial} + \sum_{i=1}^{n} \Delta a_i}{a_{transition}} \times \left[\sum_{j=1}^{n} AF_j \times \frac{\sigma_Y (local)_j}{\sigma_Y (bulk)} \right] \quad (2)$$

The proposed model has been validated on all four materials studied, and it will only be demonstrated here for the Ti-6Al-4V beta-annealed alloy.

The model relies on the knowledge of the microstructure at the location of crack initiation. Consider a two dimensional flaw (gray semicircle) with an initial size, $a_{initial}$, in the dual-phase microstructural domain of beta-annealed Ti-6Al-4V, Fig. 5(a). Since the threshold for crack propagation has been reached, according to the third assumption, the flaw will start growing at the minimum crack propagation rate of 2.54×10^{-8} mm/cycle (1×10^{-9} in/cycle), Fig. 5(b).

After N number of cycles at this crack propagation rate, the flaw will advance by an increment of Δa, which when added to the initial flaw size, $a_{initial}$, yields the current crack length, $a_{current}$. The current crack length, $a_{current}$, is then divided by the transition crack length, $a_{transition}$, to give a dimensionless value for the crack length term.

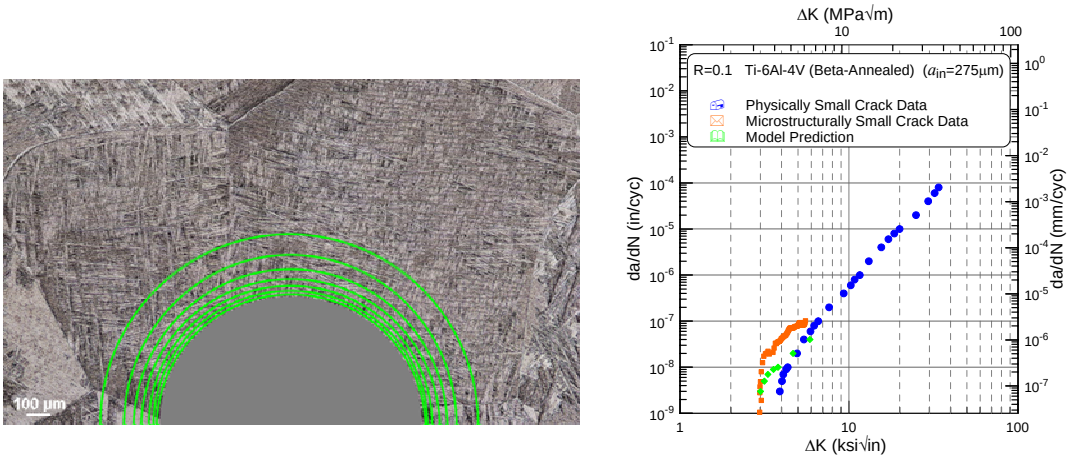

(a) (b)

Figure 5: (a) Microstructural domain of wrought Ti-6Al-4V alloy (in beta-annealed conditions) and (b) microstructurally and physically small fatigue crack growth data at R=0.1.

After N number of cycles at this crack propagation rate, the flaw will advance by an increment of Δa, which when added to the initial flaw size, $a_{initial}$, yields the current crack length, $a_{current}$. The current crack length, $a_{current}$, is then divided by the transition crack length, $a_{transition}$, to give a dimensionless value for the crack length term.

Within the crack extension increment, Δa, certain microstructural features are enveloped, Fig. 5(a). It is the resistance of these microstructural features to plastic deformation (slip) that determines the response. Thus, in the property term the relative area fractions of the microstructural features within the crack extension increment, Δa, are multiplied by their local resistance to yield, $\sigma_{Y\ (local)}$, normalized by the bulk yield strength, σ_Y. The product of the crack length and property terms provides the Ω correction to the physically small crack growth data for the crack propagation rate of interest.

As the flaw grows at gradually increasing propagation rates, the crack extension increments, Δa, are calculated and added to the initial flaw size, $a_{initial}$, in an iterative way. In parallel, the respective property terms are calculated and multiplied by the corresponding crack length terms, yielding a series of Ω corrections. This repetitive process ends when the current crack length, $a_{current}$, becomes equal to the transition crack length, $a_{transition}$, or alternatively, when the crack length term approaches unity. At this stage, the crack loses its microstructurally small character and behaves as a physically small crack.

According to Eqs. (1) and (2), the response can be predicted for any initial crack length, $a_{initial}$, and stress ratio, R. However, at very small crack sizes and high stress ratios the extent of local plasticity ahead of the crack tip (large-scale yielding) limits the use of linear elastic fracture mechanics (LEFM). The ratio of the plastic zone size, r_p, to the crack length, a, was used as a criterion to bound model's predictions [15,16]. The plastic zone size, r_p, was calculated based on the expression developed by Lados and Apelian [17], shown in Eq. (3):

$$r_p \approx (1/2\pi)^1 m\ (1/6\pi)^1 (1-m)\ \ (K_{max}{}^1 2)/(\sigma_Y{}^1 2) \qquad (3)$$

The predicted microstructurally small fatigue crack growth data are in good agreement with the experimental data, Fig. 5(b). In Fig. 6(a), the microstructurally small fatigue crack response is predicted for various positive stress ratios, R. Due to the material's high yield strength, the predicted data can be used for almost the entire range of positive stress ratios, R, Fig. 6(b).

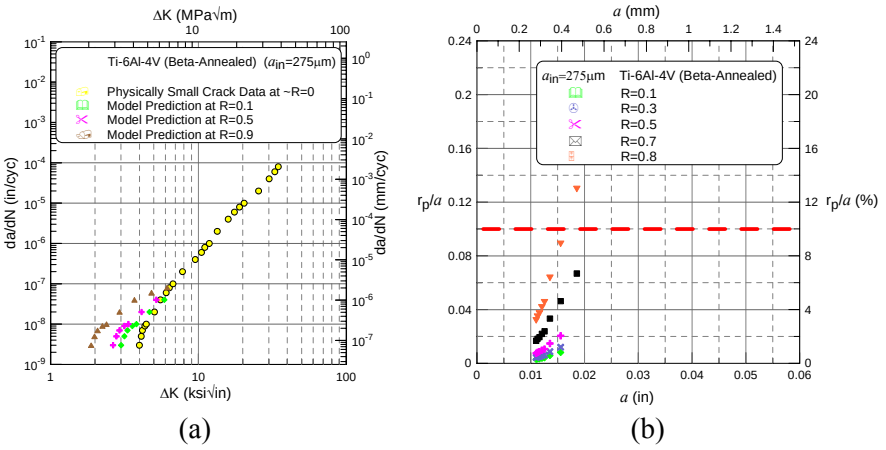

Figure 6: (a) Physically small fatigue crack growth data at ~R=0 and predicted microstructurally small fatigue crack growth data at various R, and (b) variation of r_p/a with respect to the crack size, a, at different stress ratios, R, for wrought beta-annealed Ti-6Al-4V alloy.

3.2 Two-Parameter Microstructure – Loading – Damage Mechanisms Design Maps

The new methodology introduced in Section 3.1 addresses primarily the near-threshold regime, where the differences between long and microstructurally small cracks are most prominent. In addition to the crack size, microstructure plays an important role on the fatigue crack growth threshold, and also, on the crack behavior at all growth stages. As the crack size and stress intensity factor increase, a change in the crack propagation mechanisms at the microstructure scale occurs. Based on fractographic observations, transition points from one fracture mode to another were identified for all materials studied at various R ratios, as shown on the fracture surface profiles for R=0.1, Fig. 7.

Based on these fractographic observations for various loading conditions, microstructure – loading – damage mechanisms maps were developed, Fig. 8. These maps are useful design tools, and can be used in different ways. The maps can be used for predicting the microstructural damage mechanisms for the alloys under given loading conditions (ΔK, K_{max}, and R). They can also be used to optimize materials and processes for fatigue crack growth resistance under required operating conditions. Finally, using these maps, the inspection intervals can be selected more judiciously, resulting in lower maintenance costs.

Conclusions

The findings from this work can be used for reliable fatigue life predictions, materials development and process optimization for fatigue crack growth resistance, and appropriate inspection schedules.

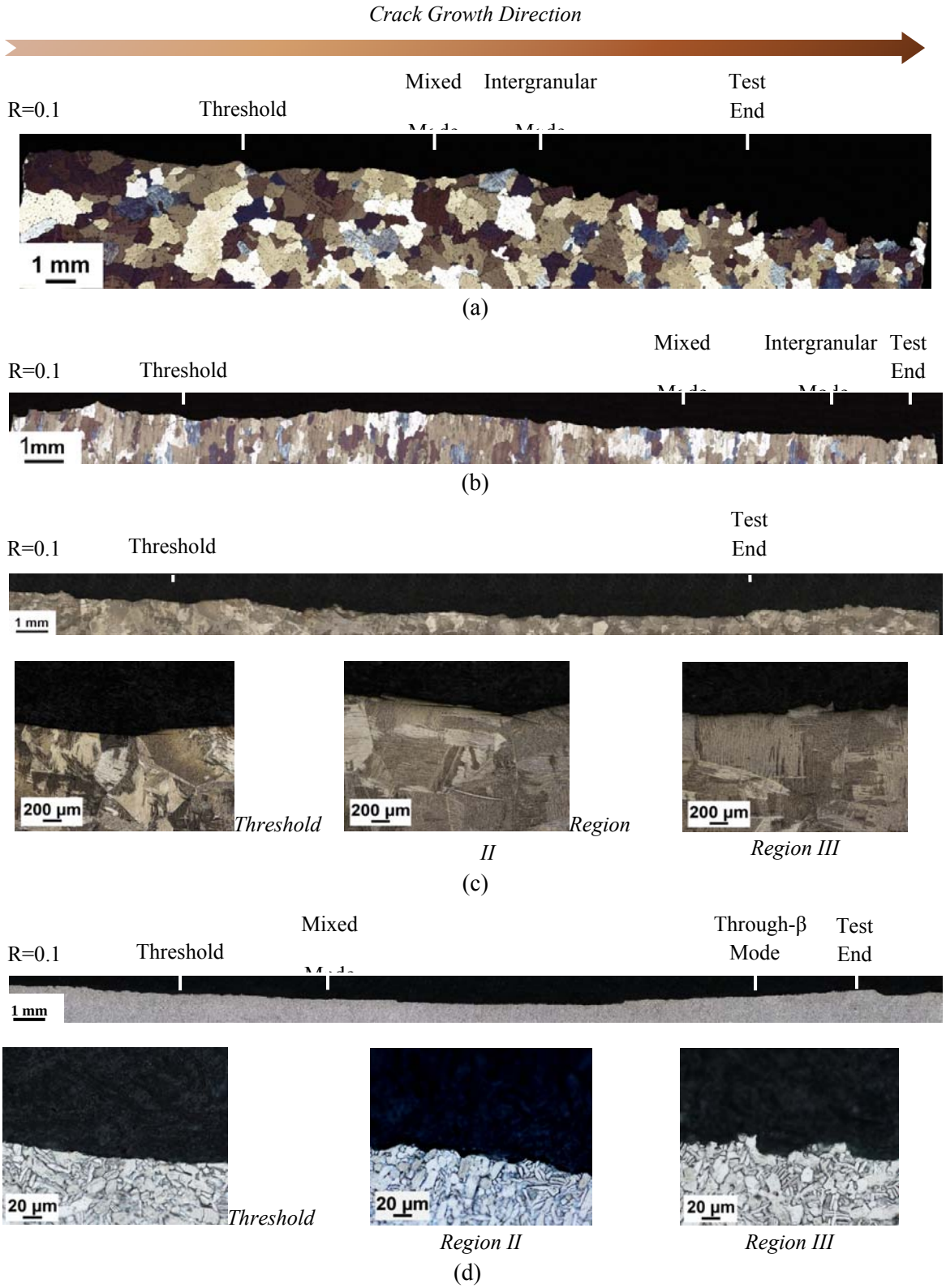

Figure 7: Fracture surface profiles of: (a) cast A535-F, (b) wrought 6061-T6, (c) beta-annealed Ti-6Al-4V, and (d) mill-annealed Ti-6Al-4V alloys tested at R=0.1.

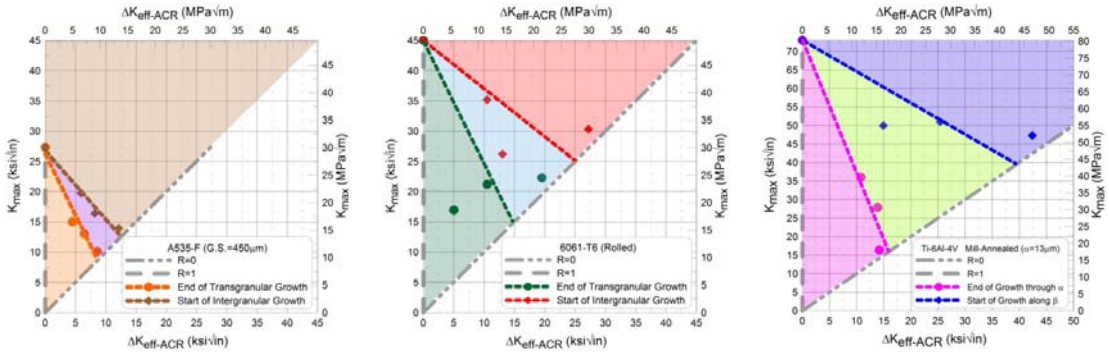

(a) (b) (c)

Figure 8: Two-parameter (ΔK–K_{max}) design maps for: (a) A535-F, (b) 6061-T6, and (c) mill-annealed Ti-6Al-4V alloys.

References

1. P.C. Paris, M.P. Gomez, W.E. Anderson, *The Trend in Engineering* **13** (1961) 9-14.
2. S. Pearson, *Eng. Fract. Mech.* **7** (1975) 235-245.
3. S. Suresh, R.O. Ritchie, *Int. Met. Rev.* **29** (6) (1984) 445–476.
4. A. Navarro, E.R. de los Rios, *Fatigue and Fract. of Engineering Materials and Structures* **11** (1987) 169-186.
5. H. Doker, V. Bachmann, G. Marci. In: *Fatigue Thresholds*. Edited by J. Backlund, A. Blom, and C. Beevers, EMAS, Warley, United Kingdom, vol. 1, pp. 45-57, 1982.
6. D.L. Davidson, *Acta Metall.* **36** (8) (1988) 2275-2282.
7. M.H. El Haddad, T.H. Topper, K.N. Smith, *Eng. Fract. Mech.* **11** (1979) 573-584.
8. N.E. Frost, D.S. Dugdale, *J. Mech. Phys. Solids* **6** (1958) 92-110.
9. M.J. Caton, J.W. Jones, J.E. Allison. In: *Fatigue Crack Growth Thresholds, Endurance Limits, and Design*. ASTM STP 1372, pp. 285-303, Edited by J.C. Newman, Jr. and R.S. Piascik, American Society for Testing and Materials, West Conshohocken, PA, 2000.
10. Y. Murakami, M. Endo, *Fracture Mechanics. 8*, Current Japanese Materials Research, H. Okamura, K. Ogura, ED., Elsevier Applied Science pub., 1990, 105-124.
11. American Society for Testing and Materials, *Standard test methods for tension testing of metallic materials*, designation E8/E8M-09; 2009.
12. S. Suresh, R.O. Ritchie, *Int. Met. Rev.* **29** (6) (1984) 445–476.
13. J.K. Donald, G.H. Bray, R.W. Bush. In: T.L. Panontin and S.D. Sheppard, editors. *Fatigue and Fracture Mechanics 29*, ASTM STP 1332. Philadelphia (PA): American Society for Testing and Materials; 674-695, 1999.
14. R.O. Ritchie, S. Suresh, *Mater. Sci. Eng. A.* **57** (1983) L27-L30.
15. ASM Handbook: *Fatigue and Fracture*, Volume 19 (1996) 374-383.
16. J. Lankford, *Fatigue and Fracture of Engineering Materials and Structures* **8** (1985) 161-175.
17. D.A. Lados, D. Apelian, *Eng. Fract. Mech.* **73** (2006) 435-455.